J|A|C|S ARTICLES

Published on Web 08/13/2010

# The Catalytic Role of N-Heterocyclic Carbene in a Metal-Free Conversion of Carbon Dioxide into Methanol: A Computational Mechanism Study

Fang Huang, Gang Lu, Lili Zhao, Haixia Li, and Zhi-Xiang Wang*

*College of Chemistry and Chemical Engineering, Graduate University of the Chinese Academy of Sciences, Beijing 100049, China*

Received April 26, 2010; E-mail: zxwang@gucas.ac.cn

***Abstract:*** A density functional theory study at the M05-2X(IEFPCM, THF)/6-311+G**//M05-2X/6-31G* level has been conducted to gain insight into the catalytic mechanism of the first metal-free N-heterocyclic carbene (NHC)-catalyzed conversion of carbon dioxide into methanol. Among the various examined reaction pathways, we found that the most favorable leads to the experimentally detected intermediates, including formoxysilane (**FOS**), bis(silyl)acetal (**BSA**), silylmethoxide (**SMO**), and disiloxane (**DSO**). However, our study also revealed that formaldehyde ($CH_2O$), generated from the dissociation of **BSA** into **DSO** and $CH_2O$ via a mechanism somewhat similar to the Brook rearrangement, should be an inevitable intermediate, although it was not reported by the experimentalists. When NHC catalyzes the reactions of $CO_2$/**FOS**/$CH_2O$ with silane, there are two activation modes. It was found that NHC prefers to activate Si−H bonds of silane and push electron density to the H atoms of the Si−H bonds in favor of transferring a hydridic atom of silane to the electrophilic C center of $CO_2$/**FOS**/$CH_2O$. This holds true in particular for the NHC-catalyzed reactions of silane with **FOS**/$CH_2O$ to produce **BSA**/**SMO**. The preferred activation mode can operate by first passing an energetically unfavorable NHC−silane local minimum via $\pi-\pi$ interactions or by directly crossing a transition state involving three components simultaneously. The activation mode involving initial coordination of NHC with the electrophilic C atom of $CO_2$/**FOS**/$CH_2O$ is less favorable or inoperable. The predicted catalytic mechanism provides a successful interpretation of the experimental observation that phenylsilane is more efficient than diphenylsilane in performing the conversion.

## 1. Introduction

Carbon dioxide ($CO_2$) causes global warming but can also be a cheap, green C1 resource. $CO_2$ fixation has attracted extensive research effort.[1−12] $CO_2$ can potentially be converted into a variety of valuable chemicals, such as formic acid and methanol.[7−12] The conversion into methanol is particularly attractive,[7c,d,10−12] because methanol can serve as an alternative to fossil fuels that may help alleviate the environmental problem and the energy crisis. While transition metal (TM)-mediated conversion of $CO_2$ into methanol has rarely been reported,[10] there have been computational and experimental explorations aimed at realizing the conversion using TM-free (or even metal-free) mediators.[11,12] Very recently, using N-heterocyclic carbenes (NHCs) as catalysts and silanes as reducing agents and hydrogen sources, Riduan, Zhang, and Ying (RZY)[12] developed the first catalytic metal-free reactions for conversion of $CO_2$ into methanol under ambient conditions (eq 1):

$$CO_2 + 3R_3SiH \xrightarrow{NHC} R_3SiOCH_3 + R_3SiOSiR_3 \qquad (1)$$
$$\xrightarrow[H_2O]{} R_3SiOH + CH_3OH$$

This approach offers a very promising chemical $CO_2$ activation and fixation protocol,[1,12] which prompted us to carry out a computational study to gain insight into the catalytic mechanism. A deep understanding may help optimize/improve the new fixation protocol. Meanwhile, the understanding of the catalytic role of NHCs in this case study may also help characterize the well-known NHC organocatalysts.[13]

## 2. Computational Details

The catalytic conversion cycle involves various weakly bonding complexes. The M05-2X density functional theory (DFT) functional was specifically developed to target nonbonding interactions.[14] In

(1) For recent reviews of $CO_2$ fixation, see: (a) Riduan, S. N.; Zhang, Y. G. *Dalton Trans.* **2010**, *39*, 3347. (b) Sakakura, T.; Kohno, K. *Chem. Commun.* **2009**, 1312. (c) Centi, G.; Perathoner, S. *Catal. Today* **2009**, *148*, 191. (d) Yu, K. M. K.; Curcic, I.; Gabriel, J.; Tsang, S. C. E. *ChemSusChem* **2008**, *1*, 893. (e) Sakakura, T.; Choi, J. C.; Yasuda, H. *Chem. Rev.* **2007**, *107*, 2365. (f) Aresta, M.; Dibenedetto, A. *Dalton Trans.* **2007**, 2975.

(2) For recent papers about $CO_2$ fixation, see: (a) Villiers, C.; Dongon, J.-P.; Pollet, R.; Thuery, P.; Ephritikhine, M. *Angew. Chem., Int. Ed.* **2010**, *49*, 3465. (b) Zhou, H.; Zhang, W. Z.; Wang, Y. M.; Qu, J. P.; Lu, X. B. *Macromolecules* **2009**, *42*, 5419. (c) Van Ausdall, B. R.; Glass, J. L.; Wiggins, K. M.; Aarif, A. M.; Louie, J. *J. Org. Chem.* **2009**, *74*, 7935. (d) Momming, C. M.; Otten, E.; Kehr, G.; Frohlich, R.; Grimme, S.; Stephan, D. W.; Erker, G. *Angew. Chem., Int. Ed.* **2009**, *48*, 6643. (e) Kayaki, Y.; Yamamoto, M.; Ikariya, T. *Angew. Chem., Int. Ed.* **2009**, *48*, 4194. (f) Dostal, L.; Jambor, R.; Ruzicka, A.; Erben, M.; Jirasko, R.; Cernoskova, E.; Holecek, J. *Organometallics* **2009**, *28*, 2633. (g) Zhou, H.; Zhang, W. Z.; Liu, C. H.; Qu, J. P.; Lu, X. B. *J. Org. Chem.* **2008**, *73*, 8039. (h) Yin, S. F.; Maruyama, J.; Yamashita, T.; Shimada, S. *Angew. Chem., Int. Ed.* **2008**, *47*, 6590. (i) Duong, H. A.; Tekavec, T. N.; Arif, A. M.; Louie, J. *Chem. Commun.* **2004**, 112.



10.1021/ja103531z 

our previous studies,[15] we also calibrated the good performance of this functional in describing weak bonding interactions. M05-2X (as implemented in Gaussian 03 program[16]) was thus selected for use in all of the DFT calculations. All of the structures were optimized and characterized as energy minima or transition states at the M05-2X/6-31G* level. The energies were then refined using M05-2X/6-311+G**//M05-2X/6-31G* single-point calculations that included solvation effects in THF solvent (one of the solvents used in the experiments) using the IEFPCM solvent model.[17] The M05-2X/6-31G* harmonic frequencies were employed for zero-point energy corrections and thermal and entropic corrections at 298.15 K and 1 atm. The free energies are used in the following discussion, unless otherwise specified, and the enthalpies are also given for reference. It should be emphasized that the entropic penalty in thermal corrections based on the ideal gas phase model are often overestimated because the gas phase model is unable to properly account for the suppressing effects of the solvent and pressure on the translational and rotational degrees of freedom of the reactants.[18] Natural bond orbital (NBO) analyses[19] at the M05-2X/6-311+G** level were performed to assign the atomic charges. Using the Molpro program,[20] we also carried out CCSD(T)/6-31G**//M05-2X/6-31G* single-point energy calculations for one reaction step to confirm the barrier evaluated by the DFT method.

## 3. Results and Discussion

RZY[12] used various NHCs and silanes to perform the conversion and proposed a mechanism (Scheme 1) on the basis of the detected species, namely, formoxysliane (**FOS**), bis(silyl)-acetal (**BSA**), silylmethoxide (**SMO**), and disiloxane (**DSO**), in their more elaborated study of the $\mathbf{NHC_{exp}}$/**DPHS**/$CO_2$ system, where $\mathbf{NHC_{exp}}$ is the 1,3-bis(2,4,6-trimethylphenyl) NHC and **DPHS** is diphenylsilane. To be computationally less costly, we chose the smaller $\mathbf{NHC_{exp}}$/**PHS**/$CO_2$ (**PHS** = phenylsilane) experimental system for our more elaborated computational study. As we will show, the use of **PHS** rather than **DPHS** does not result in essential differences in terms of the catalytic mechanism and the detected species. In fact, **PHS**


(3) For selected papers on $CO_2$ hydrosilylation studies, see: (a) Matsuo, T.; Kawaguchi, H. *J. Am. Chem. Soc.* **2006**, *128*, 12362. (b) Deglmann, P.; Ember, E.; Hofmann, P.; Pitter, S.; Walter, O. *Chem.—Eur. J.* **2007**, *13*, 2864. (c) Chung, L. W.; Lee, H. G.; Lin, Z. Y.; Wu, Y. D. *J. Org. Chem.* **2006**, *71*, 6000. (d) Jansen, A.; Pitter, S. *J. Mol. Catal. A: Chem.* **2004**, *217*, 41. (e) Jansen, A.; Gorls, H.; Pitter, S. *Organometallics* **2000**, *19*, 135. (f) Koinuma, H.; Kawakami, F.; Kato, H.; Hirai, H. *J. Chem. Soc., Chem. Commun.* **1981**, 213.

(4) For experimental studies of $CO_2$ cleavage, see: (a) Silvia, J. S.; Cummins, C. C. *J. Am. Chem. Soc.* **2010**, *132*, 2169. (b) Gu, L. Q.; Zhang, Y. G. *J. Am. Chem. Soc.* **2010**, *132*, 914. (c) van der Boom, M. E. *Angew. Chem., Int. Ed.* **2009**, *48*, 28. (d) Whited, M. T.; Grubbs, R. H. *J. Am. Chem. Soc.* **2008**, *130*, 5874. (e) Sadique, A. R.; Brennessel, W. W.; Holland, P. L. *Inorg. Chem.* **2008**, *47*, 784. (f) Laitar, D. S.; Muller, P.; Sadighi, J. P. *J. Am. Chem. Soc.* **2005**, *127*, 17196.

(5) (a) Brookes, N. J.; Ariafard, A.; Stranger, R.; Yates, B. F. *J. Am. Chem. Soc.* **2009**, *131*, 5800. (b) Zhao, H. T.; Lin, Z. Y.; Marder, T. B. *J. Am. Chem. Soc.* **2006**, *128*, 15637.

(6) (a) Correa, A.; Martin, R. *Angew. Chem., Int. Ed.* **2009**, *48*, 6201. (b) He, C.; Tian, G.; Liu, Z. W.; Feng, S. H. *Org. Lett.* **2010**, *12*, 649.

(7) For some reviews of $CO_2$ transformation into formic acid and methanol, see: (a) Jessop, P. G.; Joo, F.; Tai, C. C. *Coord. Chem. Rev.* **2004**, *248*, 2425. (b) Jessop, P. G.; Ikariya, T.; Noyori, R. *Chem. Rev.* **1995**, *95*, 259. (c) Olah, G. A.; Goeppert, A.; Prakash, G. K. S. *J. Org. Chem.* **2009**, *74*, 487. (d) Olah, G. A. *Angew. Chem., Int. Ed.* **2005**, *44*, 2636.

(8) For experimental studies of $CO_2$ transformation into formic acid, see: (a) Yasaka, Y.; Wakai, C.; Matubayasi, N.; Nakahara, M. *J. Phys. Chem. A* **2010**, *114*, 3510. (b) Sanz, S.; Benitez, M.; Peris, E. *Organometallics* **2010**, *29*, 275. (c) Zhang, Z. F.; Hu, S. Q.; Song, J. L.; Li, W. J.; Yang, G. Y.; Han, B. X. *ChemSusChem* **2009**, *2*, 234. (d) Thai, T. T.; Therrien, B.; Suss-Fink, G. *J. Organomet. Chem.* **2009**, *694*, 3973. (e) Tanaka, R.; Yamashita, M.; Nozaki, K. *J. Am. Chem. Soc.* **2009**, *131*, 14168. (f) Zhang, Z. F.; Xie, E.; Li, W. J.; Hu, S. Q.; Song, J. L.; Jiang, T.; Han, B. X. *Angew. Chem., Int. Ed.* **2008**, *47*, 1127. (g) Yin, C. Q.; Feng, Q. W.; Chen, Y.; Bai, Z. W.; Li, Z. Y. *Acta Chim. Sin.* **2007**, *65*, 722. (h) Himeda, Y.; Onozawa-Komatsuzaki, N.; Sugihara, H.; Kasuga, K. *Organometallics* **2007**, *26*, 702. (i) Himeda, Y. *Eur. J. Inorg. Chem.* **2007**, 3927. (j) Zhang, Y. P.; Fei, J. H.; Yu, Y. M.; Zheng, X. M. *Chin. Chem. Lett.* **2006**, *17*, 261. (k) Hayashi, H.; Ogo, S.; Fukuzumi, S. *Chem. Commun.* **2004**, 2714.

(9) For theoretical studies of $CO_2$ transformation into formic acid, see: (a) Urakawa, A.; Jutz, F.; Laurenczy, G.; Baiker, A. *Chem.—Eur. J.* **2007**, *13*, 3886. (b) Huang, K. W.; Han, J. H.; Musgrave, C. B.; Fujita, E. *Organometallics* **2007**, *26*, 508. (c) Ohnishi, Y. Y.; Nakao, Y.; Sato, H.; Sakaki, S. *Organometallics* **2006**, *25*, 3352. (d) Ogo, S.; Kabe, R.; Hayashi, H.; Harada, R.; Fukuzumi, S. *Dalton Trans.* **2006**, 4657. (e) Tominaga, H.; Nagai, M. *Appl. Catal., A* **2005**, *282*, 5. (f) Ohnishi, Y. Y.; Matsunaga, T.; Nakao, Y.; Sato, H.; Sakaki, S. *J. Am. Chem. Soc.* **2005**, *127*, 4021. (g) Musashi, Y.; Sakaki, S. *J. Am. Chem. Soc.* **2002**, *124*, 7588. (h) Matsubara, T. *Organometallics* **2001**, *20*, 19. (i) Musashi, Y.; Sakaki, S. *J. Am. Chem. Soc.* **2000**, *122*, 3867. (j) Pomelli, C. S.; Tomasi, J.; Sola, M. *Organometallics* **1998**, *17*, 3164. (k) Hutschka, F.; Dedieu, A.; Eichberger, M.; Fornika, R.; Leitner, W. *J. Am. Chem. Soc.* **1997**, *119*, 4432. (l) Hutschka, F.; Dedieu, A.; Leitner, W. *Angew. Chem., Int. Ed.* **1995**, *34*, 1742.

(10) Chakraborty, S.; Zhang, J.; Krause, J. A.; Guan, H. *J. Am. Chem. Soc.* **2010**, *132*, 8872.

(11) (a) Menard, G.; Stephan, D. W. *J. Am. Chem. Soc.* **2010**, *132*, 1796. (b) Ashley, A. E.; Thompson, A. L.; O'Hare, D. *Angew. Chem., Int. Ed.* **2009**, *48*, 9839. (c) Chan, B.; Radom, L. *J. Am. Chem. Soc.* **2008**, *130*, 9790. (d) Chan, B.; Radom, L. *J. Am. Chem. Soc.* **2006**, *128*, 5322.

(12) Riduan, S. N.; Zhang, Y. G.; Ying, J. Y. *Angew. Chem., Int. Ed.* **2009**, *48*, 3322.

(13) For some reviews of NHC organocatalysts, see: (a) Enders, D.; Niemeier, O.; Henseler, A. *Chem. Rev.* **2007**, *107*, 5606. (b) Marion, N.; Diez-Gonzalez, S.; Nolan, I. P. *Angew. Chem., Int. Ed.* **2007**, *46*, 2988. (c) Kamber, N. E.; Jeong, W.; Waymouth, R. M.; Pratt, R. C.; Lohmeijer, B. G. G.; Hedrick, J. L. *Chem. Rev.* **2007**, *107*, 5813. (d) Zeitler, K. *Angew. Chem., Int. Ed.* **2005**, *44*, 7506.

(14) (a) Zhao, Y.; Truhlar, D. G. *Acc. Chem. Res.* **2008**, *41*, 157. (b) Zhao, Y.; Truhlar, D. G. *J. Chem. Theory Comput.* **2006**, *2*, 1009. (c) Zhao, Y.; Schultz, N. E.; Truhlar, D. G. *J. Chem. Theory Comput.* **2006**, *2*, 364.

(15) (a) Wang, Z. X.; Lu, G.; Li, H. X.; Zhao, L. L. *Chin. Sci. Bull.* **2010**, *55*, 239. (b) Lu, G.; Li, H. X.; Zhao, L. L.; Huang, F.; Wang, Z. X. *Inorg. Chem.* **2010**, *49*, 295. (c) Jiang, J. L.; Wu, Y. B.; Wang, Z. X.; Wu, C. *J. Chem. Theory Comput.* **2010**, *6*, 1199. (d) Zhao, L.; Li, H.; Lu, G.; Wang, Z.-X. *Dalton Trans.* **2010**, *39*, 4038. (e) Li, H. X.; Zhao, L. L.; Lu, G.; Mo, Y.; Wang, Z. X. *Phys. Chem. Chem. Phys.* **2010**, *12*, 5268. (f) Li, H. X.; Zhao, L. L.; Lu, G.; Huang, F.; Wang, Z. X. *Dalton Trans.* **2010**, *39*, 5519.

(16) Frisch, M. J.; et al. *Gaussian 03*, revision E.01; Gaussian, Inc.: Wallingford, CT, 2004.

(17) (a) Sang-Aroon, W.; Ruangpornvisuti, V. *Int. J. Quantum Chem.* **2008**, *108*, 1181. (b) Tomasi, J.; Mennucci, B.; Cances, E. *THEOCHEM* **1999**, *464*, 211.

(18) (a) Zhang, C. G.; Zhang, R. W.; Wang, Z. X.; Zhou, Z.; Zhang, S. B.; Chen, Z. F. *Chem.—Eur. J.* **2009**, *15*, 5910. (b) Liang, Y.; Liu, S.; Xia, Y. Z.; Li, Y. H.; Yu, Z. X. *Chem.—Eur. J.* **2008**, *14*, 4361. (c) Chen, Y.; Ye, S.; Jiao, L.; Liang, Y.; Sinha-Mahapatra, D. K.; Herndon, J. W.; Yu, Z. X. *J. Am. Chem. Soc.* **2007**, *129*, 10773. (d) Yu, Z. X.; Houk, K. N. *J. Am. Chem. Soc.* **2003**, *125*, 13825. (e) Strajbl, M.; Sham, Y. Y.; Villa, J.; Chu, Z. T.; Warshel, A. *J. Phys. Chem. B* **2000**, *104*, 4578. (f) Hermans, J.; Wang, L. *J. Am. Chem. Soc.* **1997**, *119*, 2707. (g) Amzel, L. M. *Proteins: Struct., Funct., Genet.* **1997**, *28*, 144.

(19) (a) Reed, A. E.; Weinhold, F. *J. Chem. Phys.* **1983**, *78*, 4066. (b) Foster, J. P.; Weinhold, F. *J. Am. Chem. Soc.* **1980**, *102*, 7211. (c) Carpenter, J. E.; Weinhold, F. *THEOCHEM* **1988**, *46*, 41. (d) Glendening, E. D.; Reed, A. E.; Carpenter, J. E.; Weinhold, F. NBO, version 3.1.

(20) Ma, J.; Sun, N. N.; Zhang, X. L.; Zhao, N.; Mao, F. K.; Wei, W.; Sun, Y. H. *Catal. Today* **2009**, *148*, 221.

(21) (a) Blanrue, A.; Wilhelm, R. *Synlett* **2004**, 2621. (b) Fukuda, Y.; Kondo, K.; Aoyama, T. *Synthesis* **2006**, 2649. (c) Fukuda, Y.; Maeda, Y.; Ishii, S.; Kondo, K.; Aoyama, T. *Synthesis* **2006**, 589. (d) Kano, T.; Sasaki, K.; Konishi, T.; Mii, H.; Maruoka, K. *Tetrahedron Lett.* **2006**, *47*, 4615. (e) Song, J. J.; Gallou, F.; Reeves, J. T.; Tan, Z. L.; Yee, N. K.; Senanayake, C. H. *J. Org. Chem.* **2006**, *71*, 1273. (f) Suzuki, Y.; Bakar, A.; Muramatsu, K.; Sato, M. *Tetrahedron* **2006**, *62*, 4227.

***Scheme 1.*** Conversion Mechanism Proposed by RZY

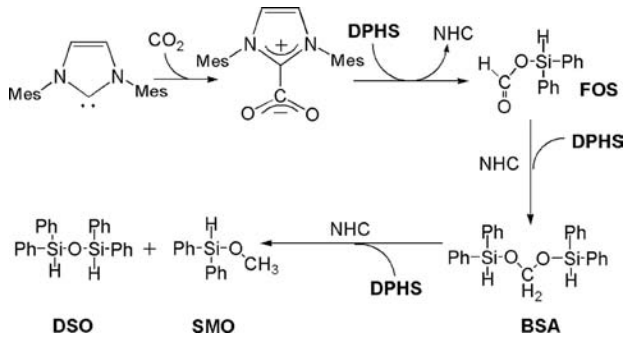


was reported to be more efficient than **DPHS** in realizing the conversion.[12]

In the study of the $\mathbf{NHC_{exp}}$/**PHS**/$CO_2$ system, we first simplified $\mathbf{NHC_{exp}}$ to 1,3-dimethyl-NHC ($\mathbf{NHC_{mod}}$) and focused on the $\mathbf{NHC_{mod}}$/**PHS**/$CO_2$ system. While the major driving forces for the reactions due to electronic effects could be captured at this layer of simplified-model calculations, using $\mathbf{NHC_{mod}}$ allowed us to consider additional possible reaction channels and obtain the reference structures of stationary points for studying the larger experimental $\mathbf{NHC_{exp}}$/**PHS**/$CO_2$ system. According to the detected species in Scheme 1, we discuss the mechanisms according to the results of the $\mathbf{NHC_{exp}}$/**PHS**/$CO_2$ system in combination with those of $\mathbf{NHC_{mod}}$/**PHS**/$CO_2$ when necessary. Full energetic and geometric results for the $\mathbf{NHC_{mod}}$/**PHS**/$CO_2$ system are provided in the Supporting Information (SI1). On the basis of the results of the $\mathbf{NHC_{exp}}$/**PHS**/$CO_2$ system, we finally examined the critical reaction steps involved in the $\mathbf{NHC_{exp}}$/**DPHS**/$CO_2$ system. It should be noted that in the DFT calculations for the two experimental systems, an ultrafine integral grid was used to improve the numerical reliability. In what follows, symbols labeled with the "mod" subscript refer to the $\mathbf{NHC_{mod}}$/**PHS**/$CO_2$ system but have characters similar to their counterparts in the $\mathbf{NHC_{exp}}$/**PHS**/$CO_2$ system.

**3.1. FOS Formation.** SAPI and SAPII in Figure 1A are the two possible reaction pathways for generating **FOS.** The optimized structures of the important stationary points along the pathways are displayed in Figure 1B. The SAPI pathway follows the reaction mechanism proposed by RZY (Scheme 1).[12] As expected, a Lewis acid−base adduct (**IM1a)** was located and found to be 7.7 kcal/mol lower than $\mathbf{NHC_{exp}}$ + $CO_2$. The donor−acceptor effect between $\mathbf{NHC_{exp}}$ and $CO_2$ weakens the C═O bonds of the $CO_2$ moiety, as shown by the elongated C═O bonds (1.236 in **IM1a** vs 1.163 Å in free $CO_2$), and results in a net charge of $-0.690e$ on the $CO_2$ moiety. The increased charge on the O atom of the $CO_2$ moiety ($-0.710e$ vs $-0.517e$ in free $CO_2$) favors attack by the carboxyl O atom of **IM1a** at the electrophilic **PHS** Si center, but the decreased charge on the C atom of the $CO_2$ moiety ($0.730e$ vs $1.034e$ in free $CO_2$) disfavors transfer of the nucleophilic **PHS** H atom to the electrophilic **IM1a** C center. After **IM1a**, the reaction can proceed concertedly or stepwise. The stepwise pathway was confirmed to be unlikely to occur in the $\mathbf{NHC_{mod}}$/**PHS**/$CO_2$ system, and we thus only considered the concerted pathway in the $\mathbf{NHC_{exp}}$/**PHS**/$CO_2$ system.

The concerted pathway proceeds via a four-membered cyclic transition state (**TS1a** in Figure 1B) that is 34.8 kcal/mol higher than the reactants ($\mathbf{NHC_{exp}}$ + **PHS** + $CO_2$). In **TS1a**, the nucleophilic **IM1a** O atom attacks the electrophilic **PHS** Si atom and the **PHS** hydridic atom (H1) approaches the electrophilic **IM1a** C1 atom. After the pathway crosses **TS1a**, intermediate **IM2a** ($\Delta G = -5.7$ kcal/mol) is formed with the well-formed Si1−O1 (1.774 Å) and C1−H1 (1.102 Å) bonds, the broken Si1−H1 bond (3.108 Å), and a formal single C1−O1 bond (1.392 Å). $\mathbf{NHC_{exp}}$ is subsequently dissociated from **IM2a** to give the detected **FOS** by crossing a barrier (**TS2a**) of 12.4 kcal/mol. The **FOS** formation step is overall exergonic by 10.3 kcal/mol.

In addition to the SAPI pathway, RZY also called attention to the possible formation of a silane−NHC adduct. While the geometry optimization to locate the $\mathbf{NHC_{mod}}$−**PHS** complex slid to separated **PHS** and $\mathbf{NHC_{mod}}$, an $\mathbf{NHC_{exp}}$−**PHS** complex (**IM3a**) could be optimized. As shown by the structure of **IM3a**, the $\pi-\pi$ stacking interaction could be responsible for its existence. Although the coordination of $\mathbf{NHC_{exp}}$ with **PHS** is thermodynamically unfavorable, it clearly implies that the reaction mode can activate **PHS** by stretching the Si−H bonds and pushing more electron density to the H atoms of the three Si−H bonds. The three Si−H bonds in **IM3a** (1.584, 1.578, and 1.509 Å) are substantially longer than the corresponding bonds in free **PHS** (1.489, 1.490, and 1.490 Å), and the charges on the three H atoms ($-0.298$, $-0.298$, and $-0.150e$) are more negative than those in **PHS** ($-0.147$, $-0.144$, and $-0.144e$). Hence, the activation mode can favor transfer of the **PHS** H atom to the $CO_2$ C center via **TS3a**, which is 4.2 kcal/mol lower than **TS1a**. On the contrary, in the $\mathbf{NHC_{mod}}$ + **PHS** + $CO_2$ reaction, which lacks such a $\pi-\pi$ interaction, the $\mathbf{TS3a_{mod}}$ barrier (30.7 kcal/mol) is 3.7 kcal/mol higher than $\mathbf{TS1a_{mod}}$. Thus a competition between the SAPI- and SAPII-like pathways can be expected for the **FOS** formation, depending on the NHC used. In the current case, the SAPII pathway is preferred. Therefore the $\pi-\pi$ interaction that can pull **PHS** and $\mathbf{NHC_{exp}}$ together is helpful but not a prerequisite for promotion of the SAPII activation mode. The reaction mode can also operate by directly crossing a transition state that involves three components (e.g., $\mathbf{NHC_{mod}}$ + **PHS** + $CO_2$) simultaneously. The intrinsic reaction coordinate (IRC) calculation (see SI2) on the $\mathbf{NHC_{mod}}$/**PHS**/$CO_2$ system indicated that the hydridic H transfer via $\mathbf{TS3a_{mod}}$ can lead to $\mathbf{IM4a_{mod}}$ directly, rather than to an ion pair as one may expect. The corresponding reaction pathway should thus occur similarly in the $\mathbf{NHC_{exp}}$/**PHS**/$CO_2$ system. $\mathbf{NHC_{exp}}$ would then be liberated from **IM4a** to give separated **FOS** + $\mathbf{NHC_{exp}}$ with a barrier (**TS4a**) of 3.8 kcal/mol. The **FOS** product formed via the SAPI and SAPII pathways has the cis conformation (see Figure 1B). It is 2.4 kcal/mol more stable than its trans isomer, which can be attributed to the favorable Coulombic attraction between electropositive Si1 and electronegative O2. In the following study of the subsequent reaction steps, we focused on the more stable cis conformation of **FOS**.

The catalytic effect of $\mathbf{NHC_{exp}}$ is significant: the barrier (**TSa** in Figure 1A) for the uncatalyzed reaction of **PHS** with $CO_2$, 47.4 kcal/mol, is much higher than **TS1a** and **TS3a**. One may ask whether the reaction step could take place more favorably than the SAPI and SAPII pathways by coordinating two $\mathbf{NHC_{exp}}$ units with $CO_2$ and **PHS** simultaneously. Because of the large size of $\mathbf{NHC_{exp}}$, we used the $\mathbf{NHC_{mod}}$/**PHS**/$CO_2$ model system to investigate the possibility. The optimized transition state ($\mathbf{TS\text{-}MOD_{syn}}$) is shown in Figure 1B. The SAPI and SAPII activation modes, which involve only single $\mathbf{NHC_{mod}}$ coordination, lower the enthalpy barriers by 35.5 and 29.8 kcal/mol, respectively, relative to the barrier for the uncatalyzed **PHS** + $CO_2$ reaction. In comparison, the activation mode with simultaneous double

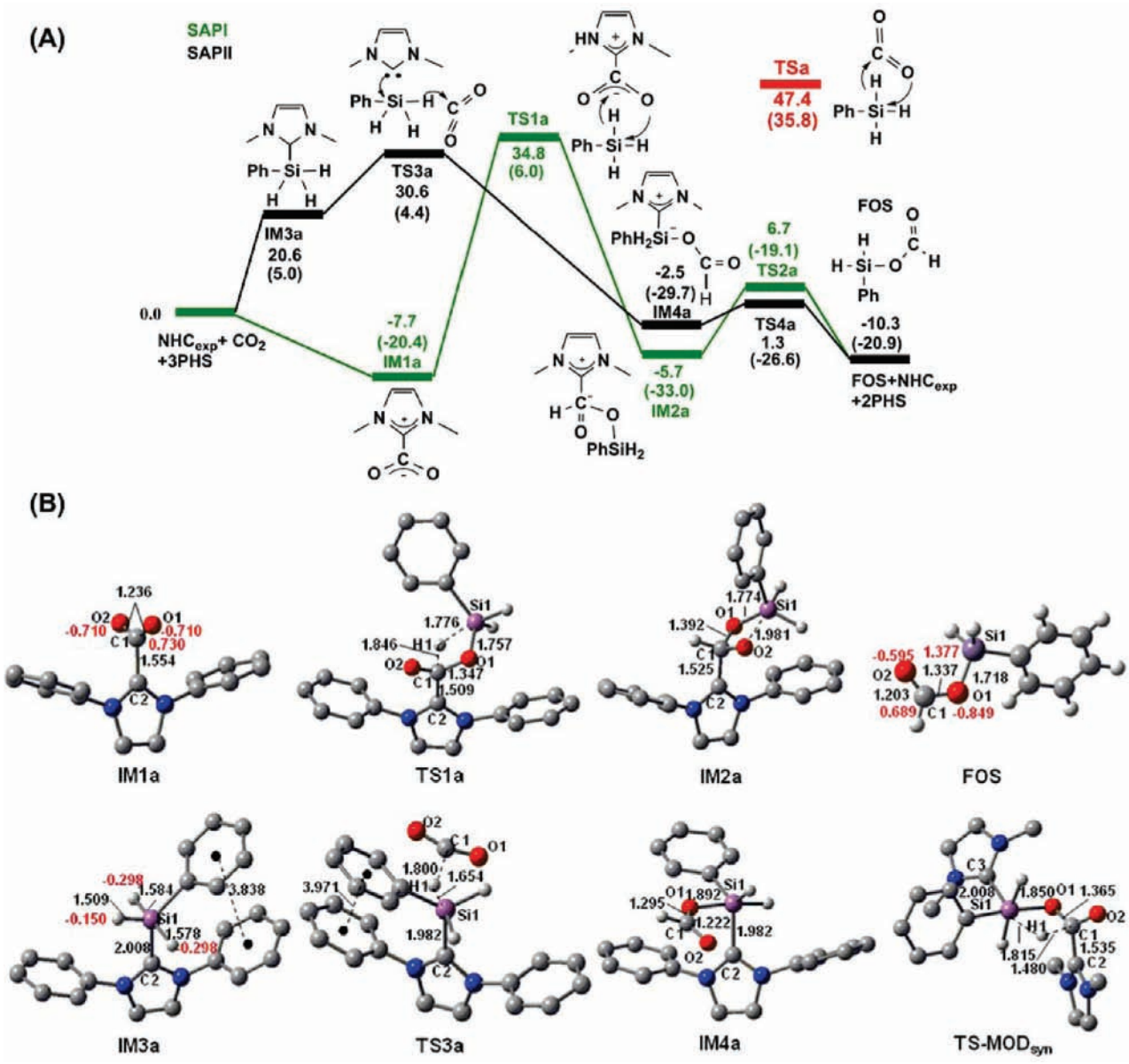


***Figure 1.*** (A) Free-energy profile (in kcal/mol) for the **FOS** formation step (values in parentheses are the corresponding enthalpies). (B) Optimized structures of the stationary points, along with the key bond lengths (black, in Å) and NBO charges (red, in *e*) used in the text (others are given in Figure S4 in section SI3 in the Supporting Information). Trivial H atoms and the methyl groups of the Mes groups of **NHC$_{exp}$** have been omitted for clarity.

**NHC$_{mod}$** coordination via **TS-MOD$_{syn}$** brings the enthalpy barrier down by 41.0 kcal/mol. However, this value is much less than the sum (35.5 + 29.8 kcal/mol) for the two separate activation modes. Therefore, the two activation modes do not operate additively. The lack of additivity can be rationalized as follows: the simultaneous coordination, on the one hand, enhances the nucleophilicities of the $CO_2$ O center and the **PHS** H center, which favors transfer of the **PHS** H atom to the $CO_2$ C center and attack by the $CO_2$ O center at the **PHS** Si center. On the other hand, the simultaneous coordination can also weaken the electrophilicities of the $CO_2$ C center and the **PHS** Si center, which disfavors transfer of the **PHS** H atom to the $CO_2$ C center and attack by the $CO_2$ O center at the **PHS** Si center. The unfavorable effects partially cancel the favorable ones. Overall, the enthalpy of the transition state (**TS-MOD$_{syn}$**) is 5.5 kcal/mol lower than that of **TS1a$_{mod}$** and 11.2 kcal/mol lower than that of **TS3a$_{mod}$** (see SI1). Nevertheless, because this reaction mode involves four components and has a larger entropic penalty than the three-component reaction, the free-energy barrier for **TS-MOD$_{syn}$** ($\Delta G^{\ddagger} = 34.1$ kcal/mol) is higher than the values of 30.7 kcal/mol (**TS3a$_{mod}$**) for SAPII$_{mod}$ and 27.0 kcal/mol (**TS1a$_{mod}$**) for SAPI$_{mod}$, indicating that the pathway via the simultaneous coordination could not be critical for **FOS** formation.

**3.2. BSA Formation.** RZY suggested that NHC catalyzes the **PHS** + **FOS** reaction to give **BSA** (Scheme 1), but it is unclear how NHC catalyzes the reaction. We considered five pathways for the **NHC$_{mod}$** + **PHS** + **FOS** reaction to give **BSA**, which are detailed in Scheme S2 in SI1; among these, the most favorable one was used to study the **NHC$_{exp}$** + **PHS** + **FOS** reaction.

The reaction pathway (black) in Figure 2A is similar to the SAPII pathway for the **FOS** formation step shown in Figure 1A. The coordination of **NHC$_{exp}$** to **PHS** activates **PHS** in favor of transferring the nucleophilic **PHS** H atom to the electrophilic **FOS** C center. However, the H transfer barrier via **TS1b** (37.6

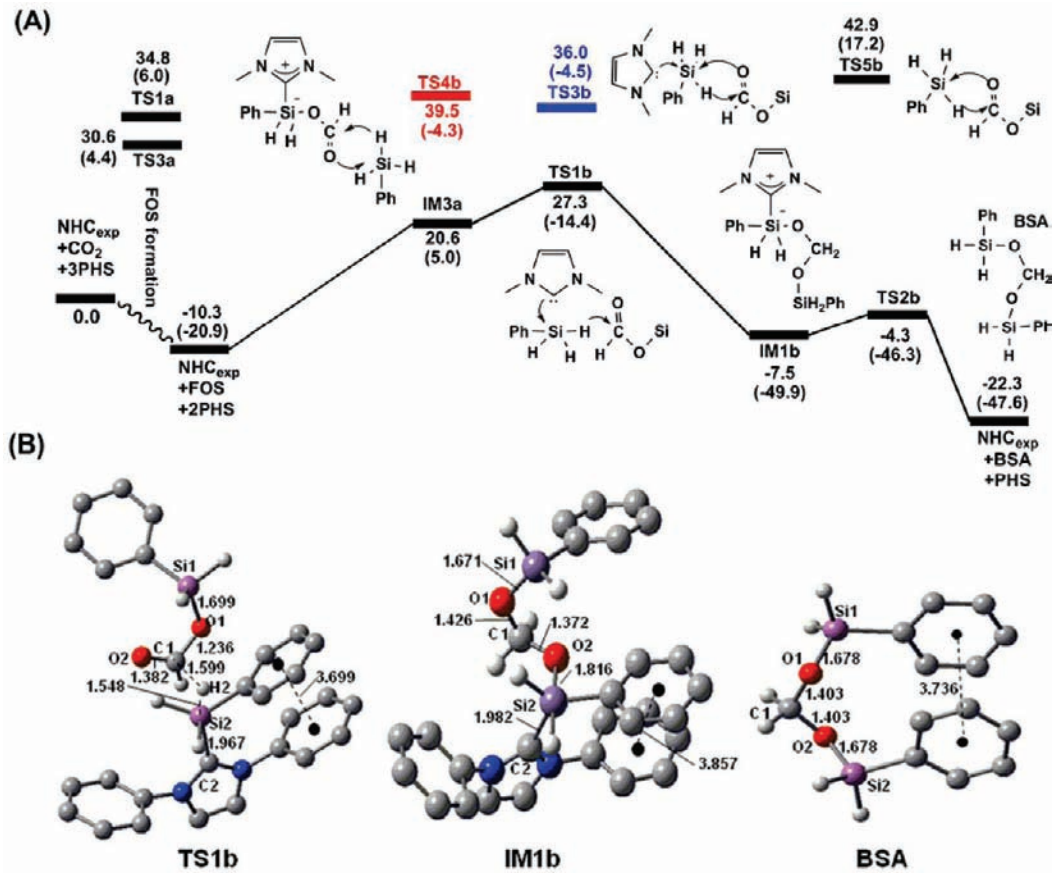


***Figure 2.*** (A) Free-energy profile (in kcal/mol) for the **BSA** formation step (values in parentheses are the corresponding enthalpies). (**B**) Optimized structures of the stationary points, along with key bond lengths (in Å) used in the text (others are given in Figure S5 in SI3). Trivial H atoms and the methyl groups of the Mes groups of $\mathbf{NHC_{exp}}$ have been omitted for clarity.

kcal/mol measured from $\mathbf{NHC_{exp}}$ + **FOS** + **PHS**) is higher than the 30.6 kcal/mol for transfer of a **PHS** H atom to $CO_2$ in the SAPII mode (see above). This is because the $CO_2$ C center is more electrophilic than the **FOS** C center, as revealed by the charges of these two C centers (1.034*e* in $CO_2$ vs 0.689*e* in **FOS**). The geometry optimization starting at an initial structure slightly away from **TS1b** could lead to the intermediate (**IM1b**) directly, which is similar to the **TS3a** → **IM4a** step in the SAPII pathway in Figure 1A and the **TS4c** → **IM2c** step (SCPa) in Figure 3A (see below) in that there is no stable ion-pair complex prior to the intermediates (**IM1b**, **IM4a**, and **IM2c**). Notably, the three reaction steps follow the same mechanism to activate **PHS**. $\mathbf{NHC_{exp}}$ can be dissociated easily from **IM1b** to give **BSA** by crossing a barrier of 3.2 kcal/mol. The uncatalyzed reaction of **PHS** + **FOS** has a barrier of 53.2 kcal/mol (**TS5b**), indicating a catalytic effect of 15.6 kcal/mol for $\mathbf{NHC_{exp}}$ with respect to the preferred reaction channel (**TS1b**).

The SAPI-like pathway in Figure 1A involving coordination of $\mathbf{NHC_{exp}}$ to **FOS** could not be located for this reaction step. Because the C1 center in **FOS** is less electropositive than its counterpart in $CO_2$ (0.689 vs 1.034*e*) and **FOS** is larger than $CO_2$, $\mathbf{NHC_{exp}}$ tends to go away during the attempt to optimize a **TS1a**-like transition state. In line with the rationalization, coordination of $\mathbf{NHC_{exp}}$ to $CO_2$ is energetically favorable by 7.7 kcal/mol, while coordination of $\mathbf{NHC_{exp}}$ to **FOS** to give **IM2a** is unfavorable by 4.6 kcal/mol (see Figure 1A).

The free-energy barrier for this step (37.6 kcal/mol, measured from $\mathbf{NHC_{exp}}$ + **FOS** + **PHS**) seems somewhat high for **BSA** formation. However, we call attention to the following aspects: (i) Because the reaction step involves three components, the predicted entropic penalty (31.1 kcal/mol, very large!) could be severely overestimated by the ideal gas phase-based model, as mentioned above. Recently, Yu and co-workers[18b] experimentally demonstrated that the gas phase model can overestimate the entropic penalty by 50−60% in their case of a two component cyclization. If a scaling factor of 0.5 is applied (noting that the reaction in the current case has three components), the scaled free-energy barrier, 22.1 kcal/mol, is in the range for experimental operation. This argument also applies to the **FOS** formation step, in which the unscaled free-energy barrier (30.6 kcal/mol, **TS3a**) is also somewhat high. (ii) The conversions are not fast, taking 4−10 h, depending on the NHC and silane used.[12] (iii) The **FOS** formation step is exergonic by 10.3 kcal/mol, which helps drive the **BSA** formation step. Notably, **TS1b** is still 3.3 kcal/mol lower than **TS3a** (see Figure 2A). When the above factors are taken into consideration, it is reasonable to conclude that the predicted mechanism for **BSA** formation is in agreement with experimental observations. Nevertheless, we further examined whether the barrier was overestimated by performing full M05-2X/6-311++G** geometry optimizations to reevaluate the barrier for the $\mathbf{NHC_{exp}}$ + **FOS** + **PHS** → **TS1b** reaction. The predicted barrier, 39.6 kcal/mol, is in reasonable agreement with the barrier of 37.6 kcal/mol predicted using the M05-2X/6-31G* structures. The other two transition states [**TS3b** (blue) and **TS4b** (red) in Figure 2A], which correspond to SBPII and SBPIII for the $\mathbf{NHC_{mod}}$/**PHS**/**FOS** system (see Scheme S2 in SI1), are less favorable than the discussed one by 8.7 and 11.6 kcal/mol, respectively.

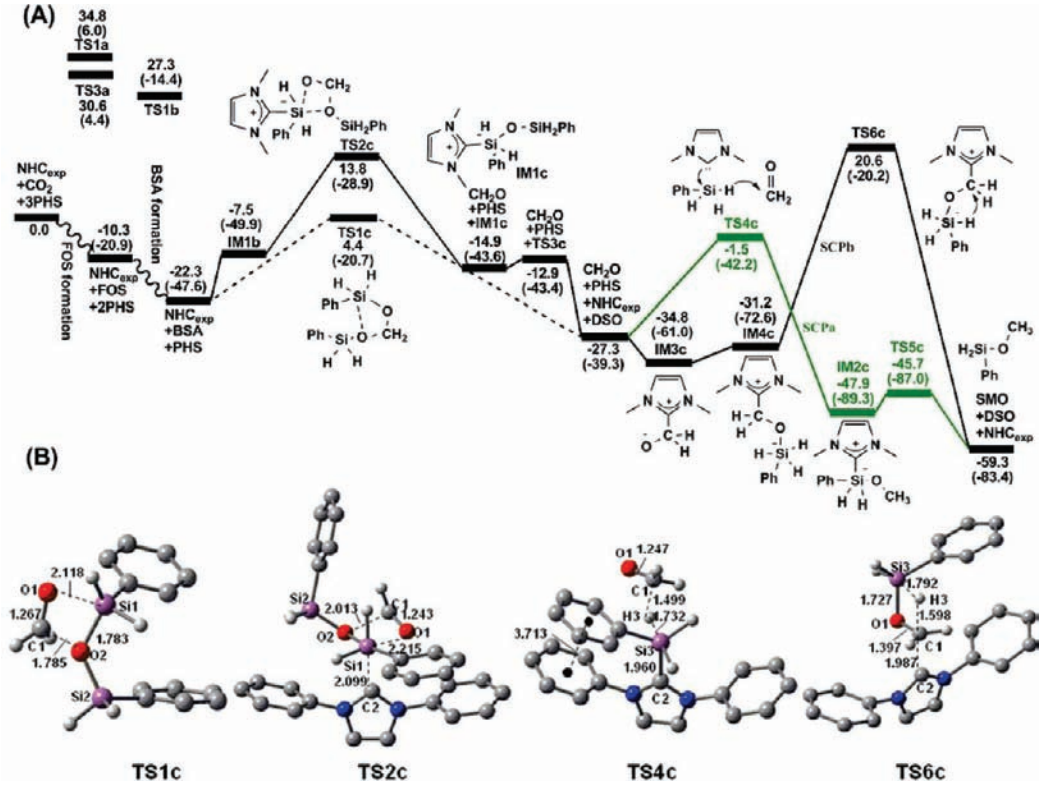


***Figure 3.*** (A) Free-energy profile (in kcal/mol) for the **SMO** formation step (values in parentheses are the corresponding enthalpies). (B) Optimized structures of some important stationary points, along with key bond lengths (in Å) used in the text (others are given in Figure S6 in SI3). Trivial H atoms and the methyl groups of the Mes groups of $\mathbf{NHC_{exp}}$ have been omitted for clarity.

**3.3. SMO Formation.** It was assumed that **BSA** reacts with a third **PHS** to generate the intermediate **SMO** through NHC catalysis. The hydrolysis of **SMO** then produces the desired methanol.[12] On the basis of the four pathways explored for the $\mathbf{NHC_{mod}}$ + **BSA** + **PHS** reaction (see Scheme S3 in SI1), the direct dissociation of **BSA** into $CH_2O$ and **DSO** (a detected species) via the transition state **TS1c** was found to be the most favorable, with a dissociation barrier of 26.7 kcal/mol. The dissociation mechanism is similar to that for the Brook rearrangement reaction (eq 2)[22] in that the nucleophilic O atom in both cases attacks the electropositive Si center. $CH_2O$ can then react with the third **PHS** via one of two possible pathways (SCPa and SCPb) to generate **SMO** (i.e., hydrosilylation of formaldehyde). In the SCPa pathway, $\mathbf{NHC_{exp}}$ activates **PHS** via a mechanism similar to those in the **FOS** (SAPII) and **BSA** formation steps. Measured from $\mathbf{NHC_{exp}}$+ **PHS** + $CH_2O$, the barrier (**TS4c**) is 25.8 kcal/mol. The SCPb pathway, which starts by coordination of $\mathbf{NHC_{exp}}$ to $CH_2O$, is similar to the SAPI pathway in the **FOS** formation step. The barrier (**TS6c**), 47.9 kcal/mol measured from $\mathbf{NHC_{exp}}$ + **PHS** + $CH_2O$, is much higher than the value of 25.8 kcal/mol for **TS4c**. Again, the $\mathbf{NHC_{exp}}$ prefers to activate the Si−H bond of **PHS** in order to transfer the electronegative **PHS** H atom to the $CH_2O$ C atom. As shown in Figure 3A, both **TS1c** and **TS4c** are lower than **TS1a**/**TS3a**/**TS1b**, indicating that the reaction to form **SMO** is thermodynamically favorable. In terms of enthalpy, coordination of $\mathbf{NHC_{exp}}$ to **BSA** can facilitate **BSA** dissociation into $CH_2O$ + **DSO** by 8.2 kcal/mol via **TS2c**. However, because the entropic penalty in the two-component reaction is larger than in the monomolecular dissociation, **TS2c** is 9.4 kcal/mol higher in free energy than the **TS1c**. After the entropic penalty is scaled by a factor of 0.5, the barrier becomes 27.4 kcal/mol, and the pathway is thus still less favorable than the direct dissociation pathway ($\Delta G^{\ddagger} = 26.7$ kcal/mol).

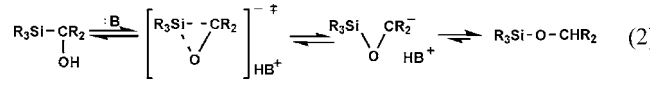

(2)

The predicted pathway for generating **SMO** is feasible, but RZY did not report the detection of $CH_2O$. To ensure that our DFT calculations did not underestimate the barrier, we reevaluated the barrier at the CCSD(T)/6-31G**//M05-2X/6-31G* level with the inclusion of a M05-2X/6-31G* free-energy correction and an M05-2X/6-311+G** solvation effect correction; the barrier, 26.6 kcal/mol, is almost the same as that predicted by the DFT method (26.7 kcal/mol). It seems that $CH_2O$ should be an inevitable intermediate, which requires further experimental verification. To support our proposed mechanism, we mention that poly-NHC particles were shown to be able to catalyze the hydrosilylation of ketone with **DPHS** in their later work (eq 3).[23]

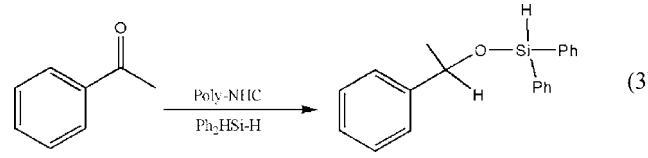

(3)

**3.4. Comparisons with the $\mathbf{NHC_{exp}}$/DPHS/$CO_2$ System.** The understanding of the $\mathbf{NHC_{exp}}$/**PHS**/$CO_2$ system allows us to

(22) (a) Brook, A. G. *Acc. Chem. Res.* **1974**, *7*, 77. (b) Smith, A. B.; Xian, M.; Kim, W. S.; Kim, D. S. *J. Am. Chem. Soc.* **2006**, *128*, 12368.

(23) Tan, M. X.; Zhang, Y. G.; Ying, J. Y. *Adv. Synth. Catal.* **2009**, *351*, 1390.

***Scheme 2.*** Energetic Comparisons between the **NHC$_{exp}$/PHS**/$CO_2$ (black) and **NHC$_{exp}$/DPHS**/$CO_2$ (red) Systems

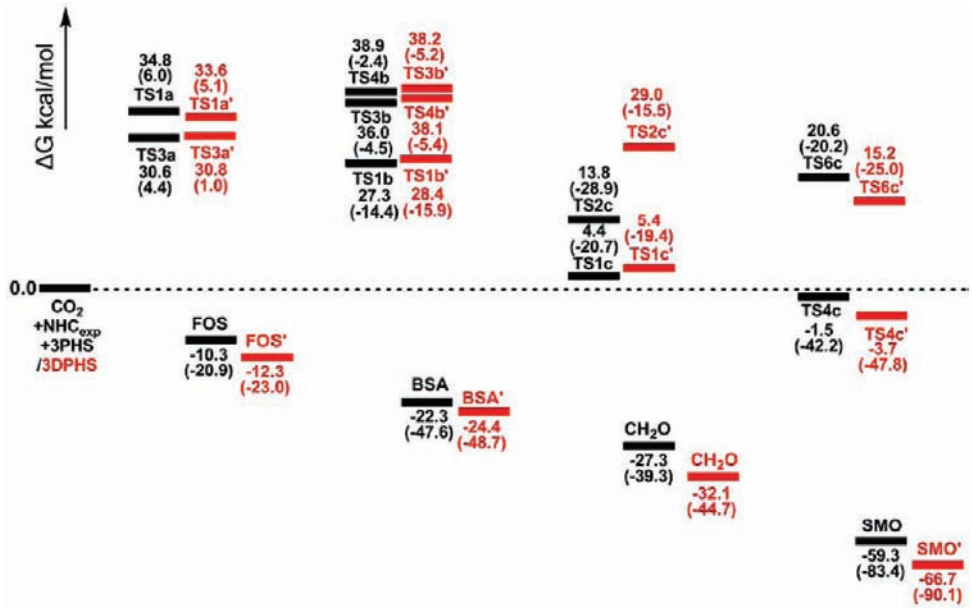


consider the larger experimental **NHC$_{exp}$/DPHS**/$CO_2$ system by focusing on the critical reaction steps. In the following, all symbols with primes refer to the stationary points in the **NHC$_{exp}$/DPHS**/$CO_2$ system. Scheme 2 compares the relative energies of the key stationary points of the two experimental systems. The optimized structures of the transition states related to the **NHC$_{exp}$/DPHS**/$CO_2$ system are displayed in Figure 4. For both systems, the reactions are downhill, driving the conversion forward thermodynamically. The comparisons indicate the following: (i) Using **DPHS** does not influence the **FOS** formation step significantly, as the relative energy of **TS3a′** (30.8 kcal/mol) is nearly equal to the value of 30.6 kcal/mol for **TS3a**,

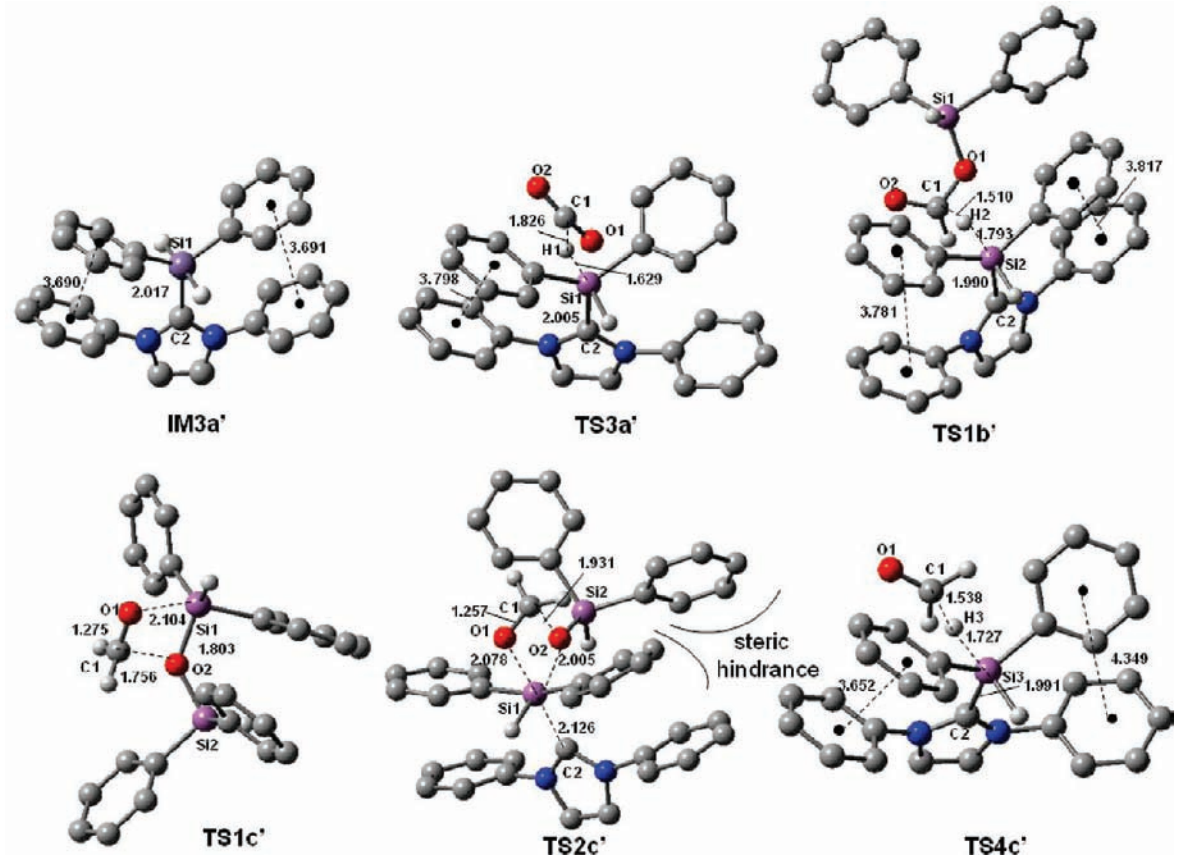


***Figure 4.*** Optimized structures of stationary points corresponding to those in Scheme 2 for the **NHC$_{exp}$/DPHS**/$CO_2$ system, along with the key bond lengths (in Å) used in the text (others are given in Figure S3 in SI5). Trivial H atoms and the methyl groups of the Mes groups of **NHC$_{exp}$** have been omitted for clarity.

although there is a difference of 1.2 kcal/mol between **TS1a′** and **TS1a**. The small influence can be attributed to the small size of $CO_2$. (ii) Similar to the **BSA** formation step in the **NHC$_{exp}$/PHS**/$CO_2$ system, the **NHC$_{exp}$** coordination with **DPHS** to give **BSA′** is also preferred. The two transition states (**TS3b′** and **TS4b′**) are 9.8 and 9.7 kcal/mol higher than **TS1b′**, respectively. (iii) In the **BSA** dissociation step for the **NHC$_{exp}$/PHS**/$CO_2$ system, the **NHC$_{exp}$** coordination with **BSA** favors the reaction enthalpically but disfavors the reaction in terms of free energy. In comparison, the **NHC$_{exp}$** coordination with **BSA′** disfavors the dissociation both enthalpically and entropically. Moreover, the energy difference (23.6 kcal/mol) between **TS1c′** and **TS2c′** is much larger than the 9.4 kcal/mol difference between **TS1c** and **TS2c**, which can be rationalized as follows: **TS2c′** and **TS2c** involve **NHC$_{exp}$**, but **TS1c′** and **TS1c** do not. Therefore, the steric effect due to the involvement of **NHC$_{exp}$** disfavors **TS2c′** more severely than **TS2c** because the **BSA′** moiety in **TS2c′** is sterically more demanding than the **BSA** moiety in **TS2c**. When the entropic penalty of the reaction step (**BSA′ → TS2c′**) is scaled, the barrier for this step is 43.3 kcal/mol, which is much higher than for **TS1c′**. Hence, the participation of **NHC$_{exp}$** severely disfavors the dissociation step of **BSA′**. (iv) Similar to the **NHC$_{exp}$**-catalyzed reaction of $CH_2O$ with **PHS**, coordination of **NHC$_{exp}$** to **DPHS** in the reaction of $CH_2O$ with **DPHS** is again preferable for promoting the reaction, as **TS6c′** is 18.9 kcal/mol higher than **TS4c′**.

According to Scheme 2, all of the subreactions in the **NHC$_{exp}$/DPHS**/$CO_2$ system are more strongly exergonic than their counterparts in the **NHC$_{exp}$/PHS**/$CO_2$ system, which implies that **DPHS** is thermodynamically more efficient than **PHS** in finishing the conversion, contrary to RZY's experimental observations. The disagreement can be reconciled by considering the absolute kinetic barriers: the absolute free-energy barriers in the **NHC$_{exp}$/DPHS**/$CO_2$ system (40.7 kcal/mol for the **FOS′ → TS1b′** step, 29.8 kcal/mol for the **BSA′ → TS1c′** step, and 28.4 kcal/mol for the $CH_2O$ → **TS4c′** step) are all larger than the corresponding values (37.6, 26.7, and 25.8 kcal/mol, respectively) in the **NHC$_{exp}$/PHS**/$CO_2$ system. As revealed by the structures of **TS1b** and **TS1b′**, the larger absolute activation barrier from **FOS′** to **TS1b′** (40.7 kcal/mol vs 37.6 kcal/mol from **FOS** to **TS1b**) is mainly due to the steric effect between the additional phenyl groups of the two **DPHS**. In the transition state **TS4c′**, the involvement of $CH_2O$ distorts one of the two $\pi-\pi$ interactions in comparison with **IM3a′** (i.e., the **NHC$_{exp}$−DPHS** complex) (Figure 4), resulting in an unfavorable steric effect. In contrast, the $CH_2O$ involvement in **TS4c** does not influence the $\pi-\pi$ interaction significantly; both **TS4c** and **IM3a** (i.e., the **NHC$_{exp}$−PHS** complex) contain one $\pi-\pi$ interaction. The difference due to the $CH_2O$ involvement explains why the barrier of 28.4 kcal/mol from $CH_2O$ to **TS4c′** is larger than the 25.8 kcal/mol barrier from $CH_2O$ to **TS4c**.

**3.5. Catalytic Character of NHCs.** NHCs are well-known organocatalysts.[13] This case study provides good examples for characterizing NHC organocatalysts. The nine NHC-catalyzed reactions (i.e., the three **NHC$_{mod}$**-catalyzed reactions $CO_2$/**FOS**/$CH_2O$ + **PHS** and the six **NHC$_{exp}$**-catalyzed reactions $CO_2$ + **PHS**/**DPHS**, **FOS** + **PHS**/**FOS′** + **DPHS**, and $CH_2O$ + **PHS**/**DPHS**) are mostly relevant to the previously reported 1,2-additions of silanes[23]/$TMSCF_3$[24]/TMSCN[21] to ketones/aldehydes. Two activation modes have been proposed to rationalize these 1,2-additions. The NHC can first coordinate with the ketone/aldehyde by forming a complex (mode A) or activate the silane Si−H bond[23]/$TMSCF_3$ Si−$CF_3$ bond[24]/TMSCN Si−CN bond[21] (mode B). While both modes have been assumed for aldehyde 1,2-additions, only mode B has been applied to ketone 1,2-additions because ketones are more sterically demanding than aldehydes, making formation of complexes with NHCs difficult.

***Scheme 3.*** Comparison of the Two Activation Modes

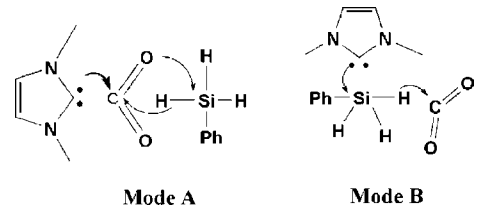


***Table 1.*** Comparison of Activation Modes A and B

| | | mode A | | mode B | |
|---|---|---|---|---|---|
| entry | reaction | complex ($\Delta G$)[a] | TS ($\Delta G^{\ddagger}$)[b] | complex ($\Delta G$)[a] | TS ($\Delta G^{\ddagger}$)[b] |
| 1 | **NHC$_{mod}$** + **PHS** + $CO_2$ | −11.8 | 27.0 | −[c] | 30.7 |
| 2 | **NHC$_{mod}$** + **PHS** + **FOS** | 5.4 | − | − | 37.6 |
| 3 | **NHC$_{mod}$** + **PHS** + $CH_2O$ | −6.5 | 45.5 | − | 28.4 |
| 4 | **NHC$_{exp}$** + **PHS** + $CO_2$ | −7.7 | 34.8 | 20.6 | 30.6 |
| 5 | **NHC$_{exp}$** + **PHS** + **FOS** | 4.6 | − | 20.6 | 37.6 |
| 6 | **NHC$_{exp}$** + **PHS** + $CH_2O$ | −7.5 | 47.9 | 20.6 | 25.8 |
| 7 | **NHC$_{exp}$** + **DPHS** + $CO_2$ | −7.7 | 33.6 | 16.7 | 30.8 |
| 8 | **NHC$_{exp}$** + **DPHS** + **FOS′** | 5.8 | − | 16.7 | 40.7 |
| 9 | **NHC$_{exp}$** + **DPHS** + $CH_2O$ | −7.5 | 47.3 | 16.7 | 28.4 |

[a] Binding free energies (in kcal/mol) of NHC−$CO_2$/**FOS**/$CH_2O$ relative to NHC + $CO_2$/**FOS**/$CH_2O$. [b] Binding free energies (in kcal/mol) of NHC−**PHS**/**DPHS** complexes relative to NHC + **PHS**/**DPHS**. [c] No transition states or complexes.

Using the **NHC$_{exp}$**-catalyzed **PHS** + $CO_2$ reaction as an example, Scheme 3 illustrates the two activation modes. Table 1 compares the energetics of the two activation modes. When the nine reactions are taken into account, the comparisons reveal the following: (i) Mode A activation is operable only if there exist complexes (entries 1, 3, 4, 6, 7, and 9) with certain stability (negative binding free energies). For entries 2, 5, and 8, although the complexes could be optimized, the complexes are unstable with positive binding free energies, and the transition states could not be located. (ii) In contrast to mode A, mode B is always operable regardless of whether there exist complexes prior to the transition states. Furthermore, mode B activation tends to be preferable over mode A activation except for entry 1, although $CO_2$ and $CH_2O$ are less sterically demanding than aldehydes and can form stable complexes with **NHC$_{exp}$**. Using the NHC-catalyzed $CO_2$ + **PHS** reaction as an example (see Scheme 3), we rationalize the preference as follows: For mode A activation, NHC coordination to $CO_2$ favors attack by the electronegative O atom of $CO_2$ at the electropositive **PHS** Si center but simultaneously disfavors the H transfer from **PHS** to $CO_2$ because the coordination renders the $CO_2$ C atom less electropositive and the $CO_2$ O atom more electronegative. The unfavorable effect partially cancels the favorable one. In mode B activation, the NHC attacks the **PHS** Si center, which activates the Si−H bond and simultaneously pushes more negative charge to the **PHS** H atoms. Both effects are favorable for the H transfer from **PHS** to $CO_2$. Nevertheless, a systematic investigation is apparently required in order to examine whether these observations apply to other NHC-catalyzed hydrosilylation/hydrosilylation-like reactions.

(24) Song, J. J.; Tan, Z. L.; Reeves, J. T.; Gallou, F.; Yee, N. K.; Senanayake, C. H. *Org. Lett.* **2005**, *7*, 2193.

***Scheme 4.*** Detailed Mechanism of the Whole Catalytic Cycle[a]

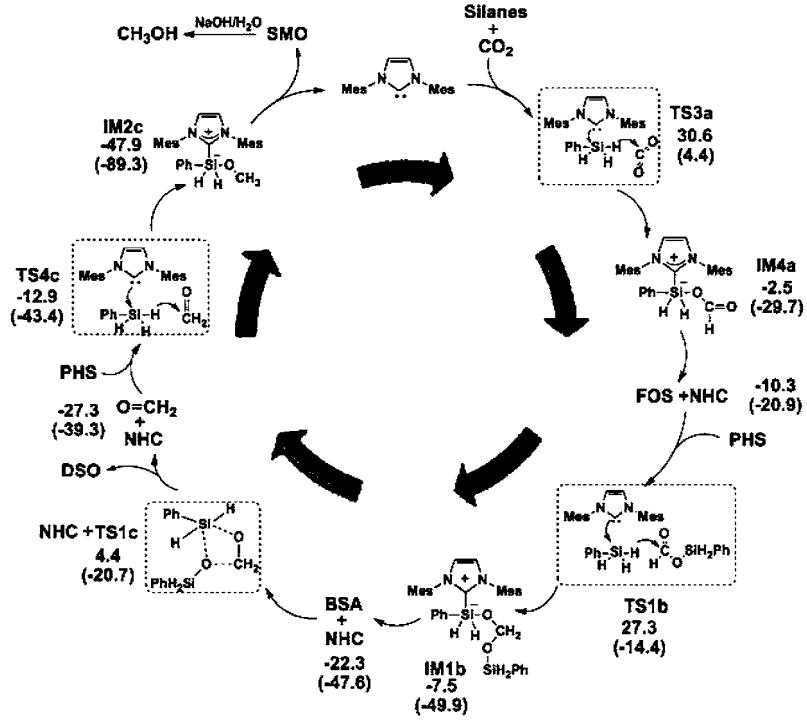


[a] The values below the names of the stationary points are the free energies and entropies (in parentheses) relative to $\mathbf{NHC}_{exp} + 3\mathbf{PHS} + CO_2$.

## 4. Conclusions

The results of the computational study have allowed us to detail the mechanism of the entire catalytic cycle in Scheme 4. The predicted mechanism successfully rationalizes the experimental detection of the intermediates (**FOS**, **BSA**, **SMO**, and **DSO**). However, $CH_2O$ is predicted to be an inevitable intermediate, which still requires experimental verification. The energetic results indicate that NHC prefers to activate the Si−H bond of silanes, favoring transfer of one of the hydridic atoms of the silane to the positively charged C center of $CO_2$/**FOS**/$CH_2O$. The activation mode involving prior coordination of NHC to the electrophilic carbon center is energetically less favorable or inoperable. In the case of $\mathbf{NHC}_{exp}$ catalysis in the $CO_2$/**FOS**/$CH_2O$ system, there is a local minimum prior to the transition state. Although the complex is energetically unfavorable relative to separated $\mathbf{NHC}_{exp} + \mathbf{PHS}$, the complex is helpful in promoting the preferred activation mode by pulling $\mathbf{NHC}_{exp}$ and **PHS** together. Nevertheless, the formation of such a complex is not a prerequisite for promotion of the activation mode. The mode can operate via a transition state involving three components simultaneously. The role of NHC is indeed amazing. It is always there when needed and then leaves when its mission is accomplished.

**Acknowledgment.** This work was supported financially by funds from the Chinese Academy of Sciences and the NSFC (Grants 20973197 and 20773160). We thank the referees for constructive suggestions to improve the work and Professor Rainer Glaser for reading the manuscript and helpful discussions.

**Supporting Information Available:** Full geometric and energetic results for the $\mathbf{NHC}_{mod}$/$CO_2$/**PHS** system (SI1), IRC results (SI2), optimized structures of all stationary points in Figures 1−4 (SI3), complete ref 16 (SI4), and total energies and Cartesian coordinates of all the structures (SI5). This material is available free of charge via the Internet at http://pubs.acs.org.

JA103531Z